Interfacial Electron Redistribution of FeCo2S4/N-S-rGO Boosting Bifunctional Oxygen Electrocatalysis Performance

Wen-Lin Zhang, Shi-Meng Liu, Lu-Hua Zhang, Ting-Ting He and Feng-Shou Yu *

National-Local Joint Engineering Laboratory for Energy Conservation in Chemical Process Integration and Resources Utilization, School of Chemical Engineering and Technology, Hebei University of Technology, Tianjin 300130, China

* Correspondence: yfsh@hebut.edu.cn

1 Materials and Methods

1.1 Materials

All reagents are commercially available and used without further purification. rGO was obtained from Chengdu Zhongke Times Naneng Technology Co., Ltd. Iron (III) nitrate nonahydrate ($Fe(NO_3)_3 \cdot 9H_2O$, 98.5%), cobalt (II) nitrate hexahydrate ($Co(NO_3)_2 \cdot 6H_2O$, 98.5%), ammonium fluoride (NH_4F, 96%), urea ($CO(NH_2)_2$, AR), thiourea (CH_4N_2S, AR), Sulfur sublimed (S, ≥99.5%), Sodium sulfide (Na_2S), were purchased from Bide Pharmatech Ltd. Conductive carbon black, Nafion solution ($C_9HF_{17}O_5F$, 5wt.%), were purchased from Kunshan Yiersheng Energy Co., Ltd.

1.2 Synthesis of N-S-rGO

The N-S-rGO substrate was obtained by mixing and grinding 0.01 g of rGO with 0.15 g of thiourea and pyrolyzing the mixture at 800 °C for 1 h under N_2 atmosphere. The N-rGO and S-rGO were synthesized in the same method with urea and sulfur powder as N and S sources, respectively.

1.3 Electrochemical measurements

ORR tests were performed in 0.1 M KOH and the electrolyte needed to be purged with O_2 for at least 30 min prior to the measurement. Cyclic voltammetry (CV) measurements were performed in O_2 saturated 0.1 M KOH by first measuring 60 cycles at a scan rate of 100 mV s^{-1} and then at a scan rate of 5 mV s^{-1} for test to obtain polarization curves. In control experiments, CV measurements were performed under N_2 atmosphere. The catalytic activity was measured by linear sweep voltammetry (LSV) at 400, 625, 900, 1225, 1600, 2025 rpm with a scan rate of 5 mV s^{-1}, and the potential was set from 1.21 to 0.00 V vs RHE. The CHI760E electrochemical workstation with a three-electrode system was used to evaluate the electrochemical properties of ORR and OER in an O_2 saturated KOH electrolyte (0.1 M, 20 °C). All measurements initially versus Hg/HgCl and then were referred versus the RHE according to the Nernst equation:

$$E_{RHE} = E_{Hg/HgCl} + 0.244 + 0.0592 \times pH \qquad (S1)$$

Rotating ring-disk electrode (RRDE) measurements were performed at a scan rate of 5 mV s^{-1} at 1600 rpm, and the ring electrode voltage was kept at 1.3 V (vs. RHE).

The stability tests were implemented through current-time (i-t) chronoamperometric responses for 25000 s and methanol tolerance tests were collected by i-t response at the above potential with 4 mL methanol (3 M) addition at 400 s.

The OER catalytic activities were recorded in an O_2-saturated 0.1 M KOH solution by CV and LSV curves with a scan rate of 5 mV s^{-1} in the potential range of 1.00 V to 2.01 V (vs RHE), corrected by iR-compensation. Besides, the rotating speeds for OER was fixed to 1600 rpm to remove the oxygen bubble released during the reacting process. And before actual measurements, 60 CV cycles were conducted to obtain stable experimental data.

The polarization curves of all prepared samples were captured using the same rotation speed.
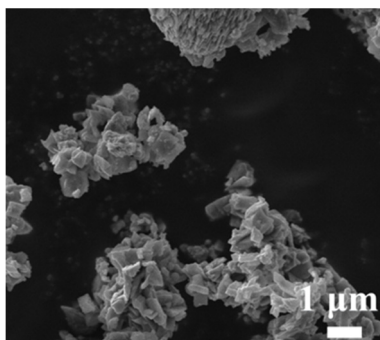
**Figure S1.** SEM images of FeCo$_2$S$_4$
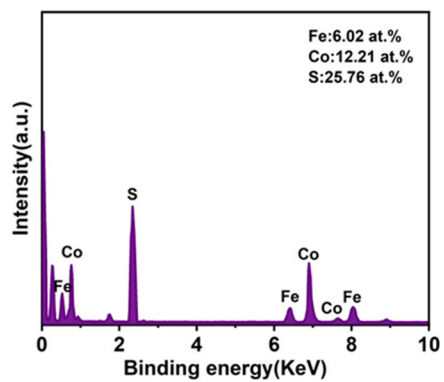
**Figure S2.** EDS data of FeCo$_2$S$_4$/N-S-rGO
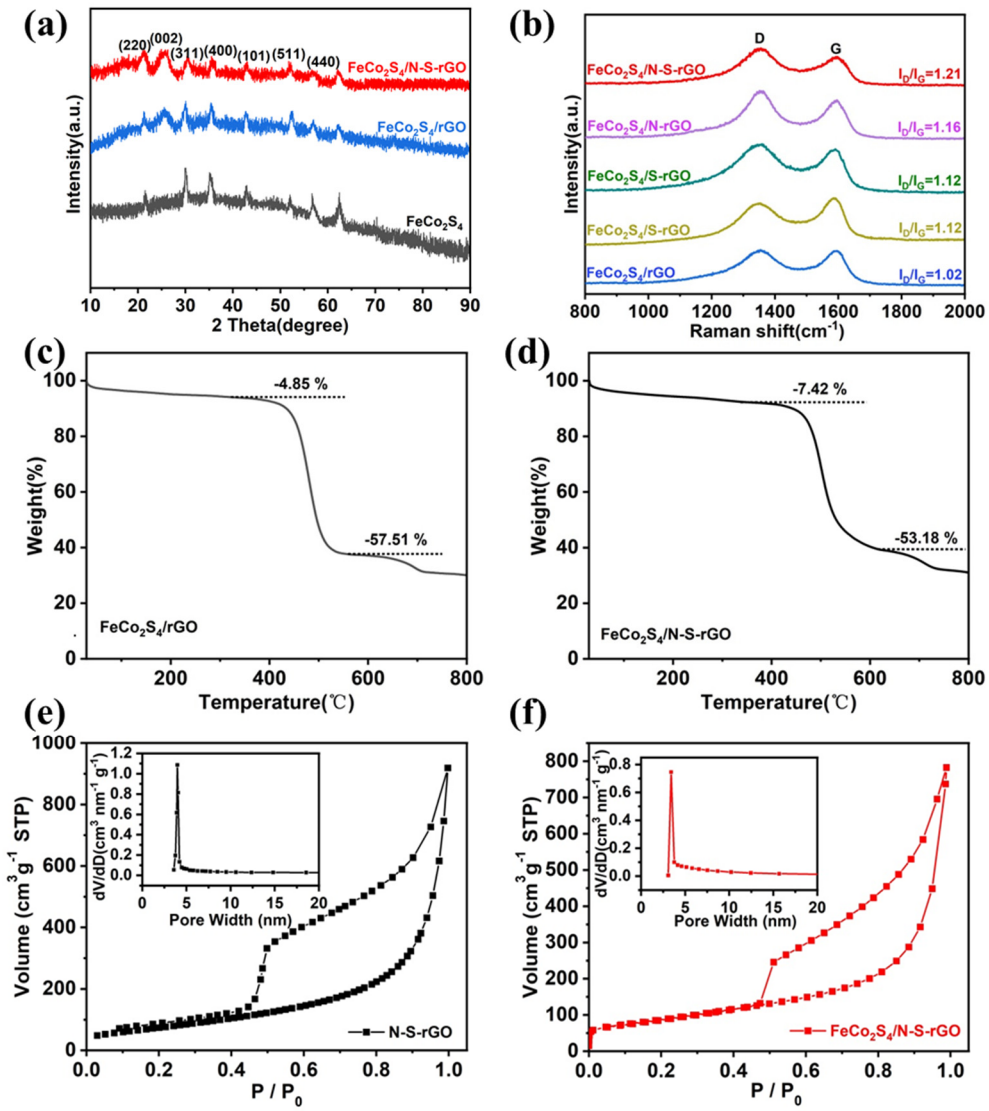
Figure S3. (a) XRD pattern; (b) Raman pattern; (c, d) TG curves of FeCo₂S₄/rGO and FeCo₂S₄/N-S-rGO in air atmosphere; (e, f) nitrogen adsorption-desorption isotherms and pore size distribution of FeCo₂S₄/N-S-rGO and N-S-rGO.
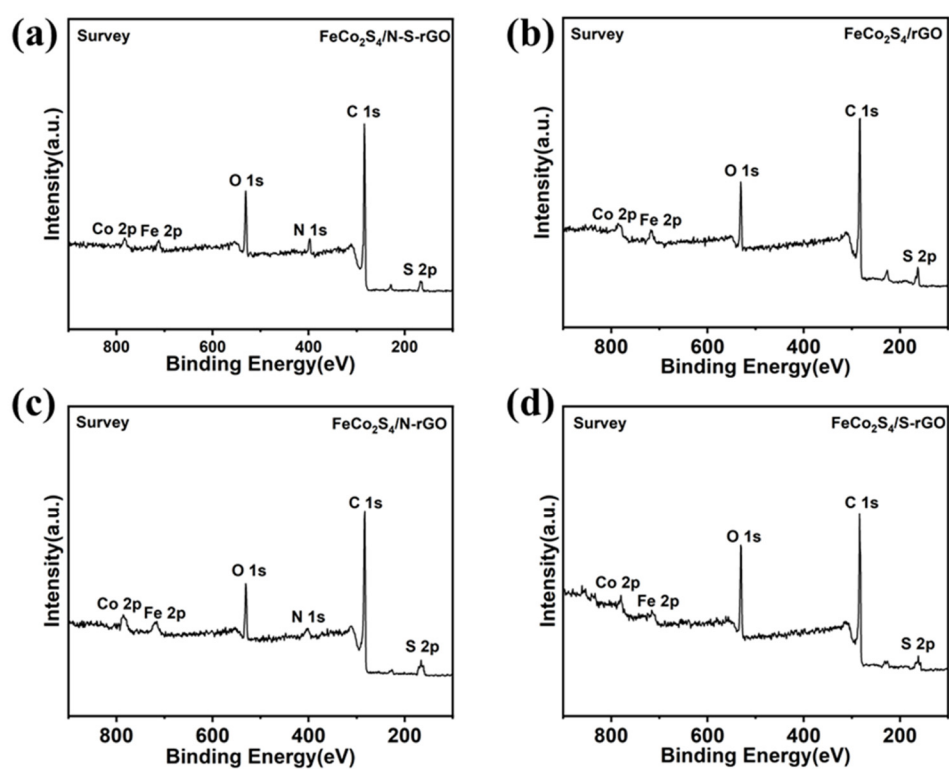
Figure S4. (a) Total XPS profiles for FeCo$_2$S$_4$/N-S-rGO. (b) total XPS profiles for FeCo$_2$S$_4$/rGO. (c) total XPS profiles for FeCo$_2$S$_4$/N-rGO. (d) total XPS profiles for FeCo$_2$S$_4$/S-rGO.
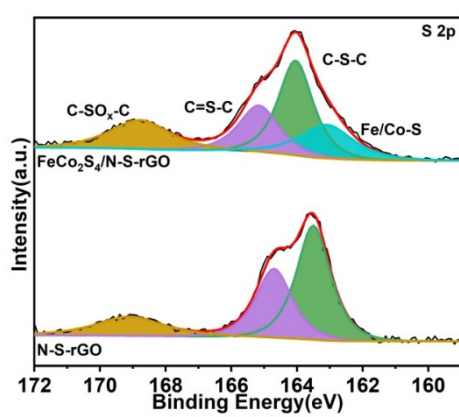
Figure S5. Fine XPS patterns of S 2p for FeCo$_2$S$_4$/N-S-rGO and FeCo$_2$S$_4$/rGO.
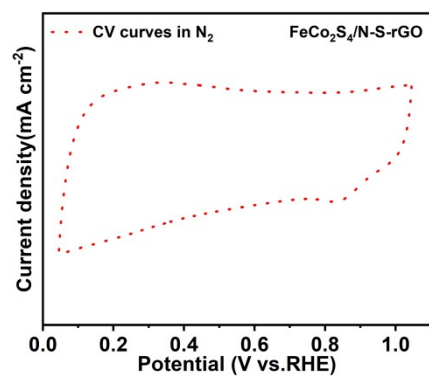
**Figure S6.** CV curves of FeCo2S4/N-S-rGO in N2 saturated 0.1 M KOH.
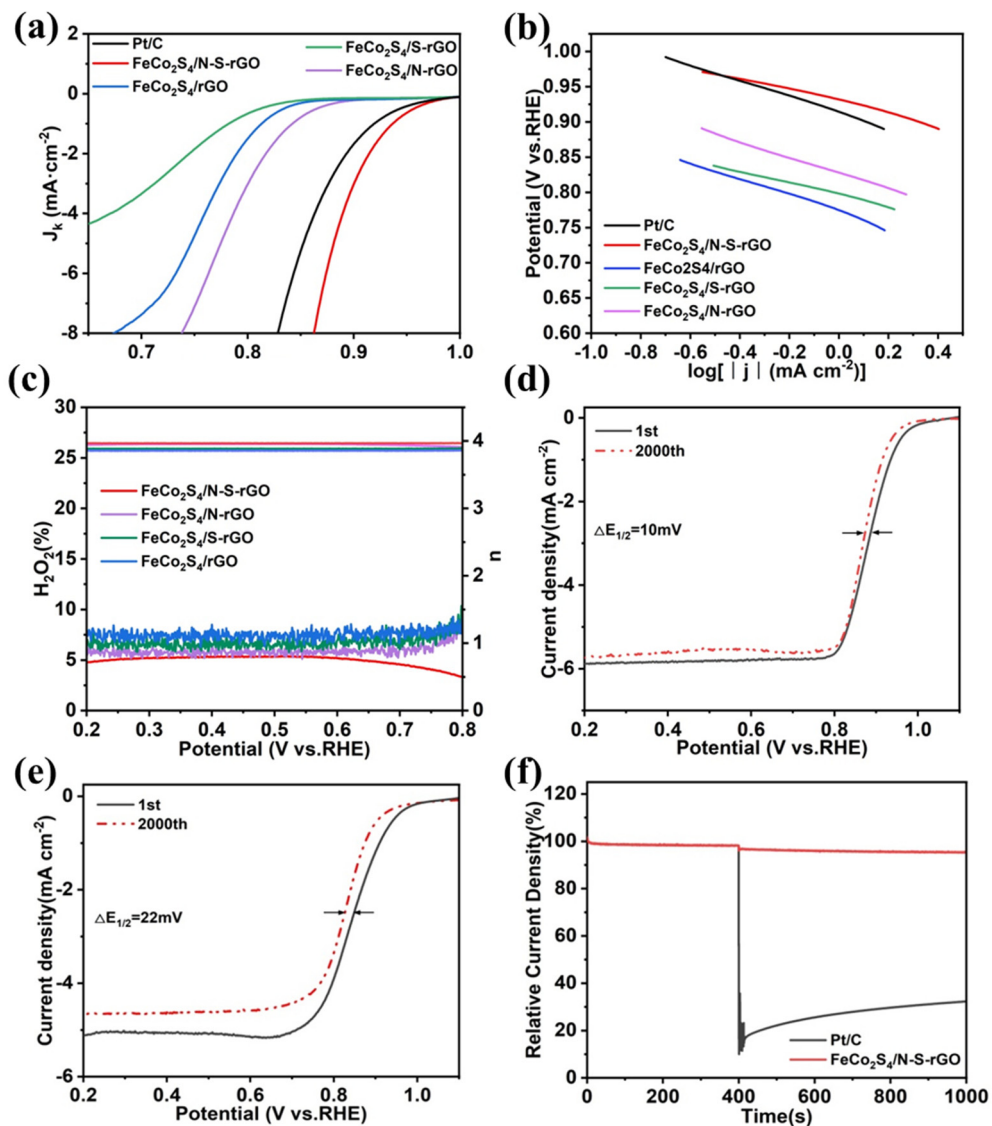
Figure S7. (a) Kinetic current density (J_K) curves of different catalysts; (b) tafel slope plots for different catalysts; (c) comparison of the number of transferred electrons (n) and the yield of the side reaction hydrogen peroxide (H_2O_2%) calculated in the RRDE test for different catalysts; (d) LSV curves of $FeCo_2S_4$/N-S-rGO versus after 2000 cycles of CV; (e) LSV curves of Pt/C (20 wt.%) versus after 2000 cycles of CV; (f) methanol tolerance test of Pt/C (20wt.%) and $FeCo_2S_4$/N-S-rGO.
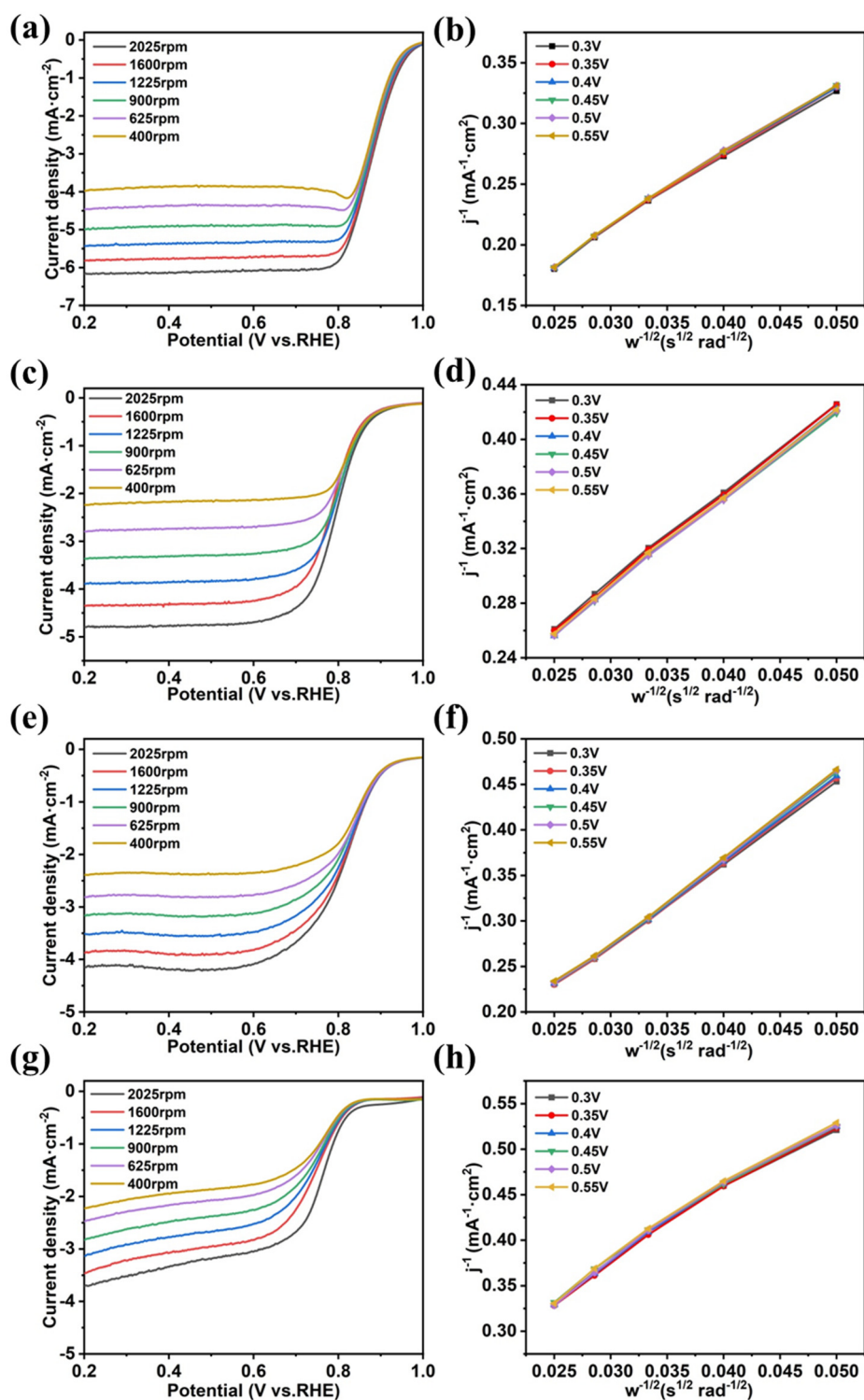
Figure S8. (a, c, e, g) ORR curves of the FeCo$_2$S$_4$/N-S-rGO, FeCo$_2$S$_4$/N-rGO, FeCo$_2$S$_4$/S-rGO, FeCo$_2$S$_4$/rGO at different rotation rates (400, 625, 900, 1225, 1600, 2025 rpm); (b, d, f, h) K-L curves of FeCo$_2$S$_4$/N-S-rGO, FeCo$_2$S$_4$/N-rGO, FeCo$_2$S$_4$/S-rGO, FeCo$_2$S$_4$/rGO calculated by the K-L equation.
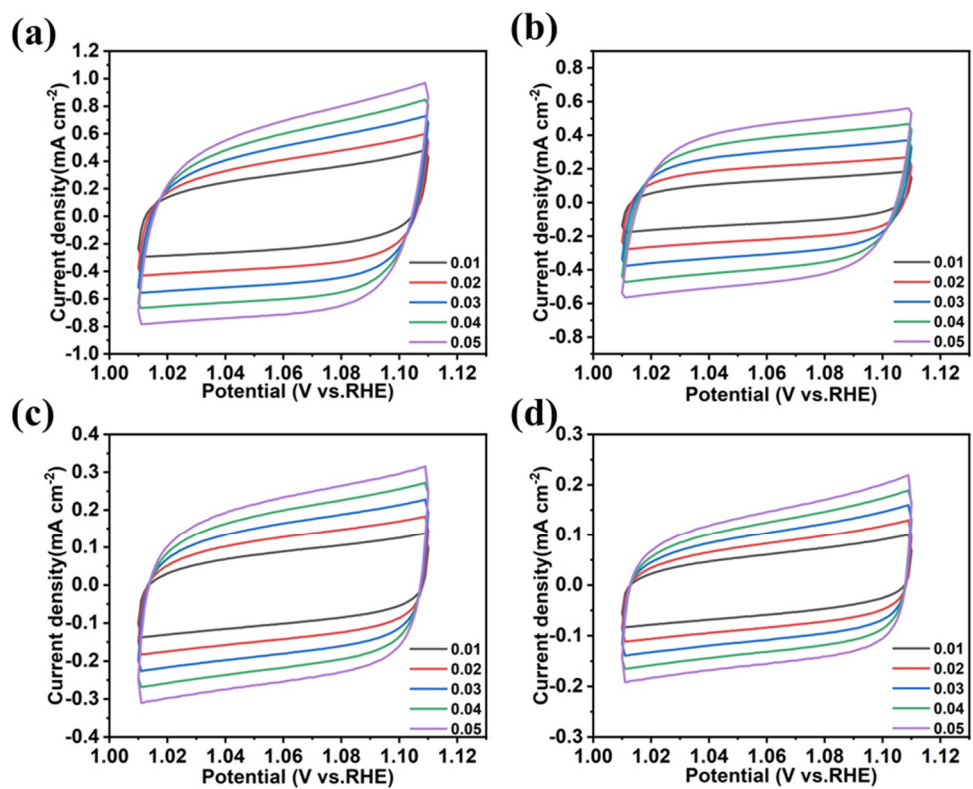
Figure S9. CV curves of the (a) $FeCo_2S_4$/N-S-rGO; (b) $FeCo_2S_4$/N-rGO; (c) $FeCo_2S_4$/S-rGO and (d) $FeCo_2S_4$/rGO recorded at 10, 20, 30, 40 and 50 mV s^{-1}.
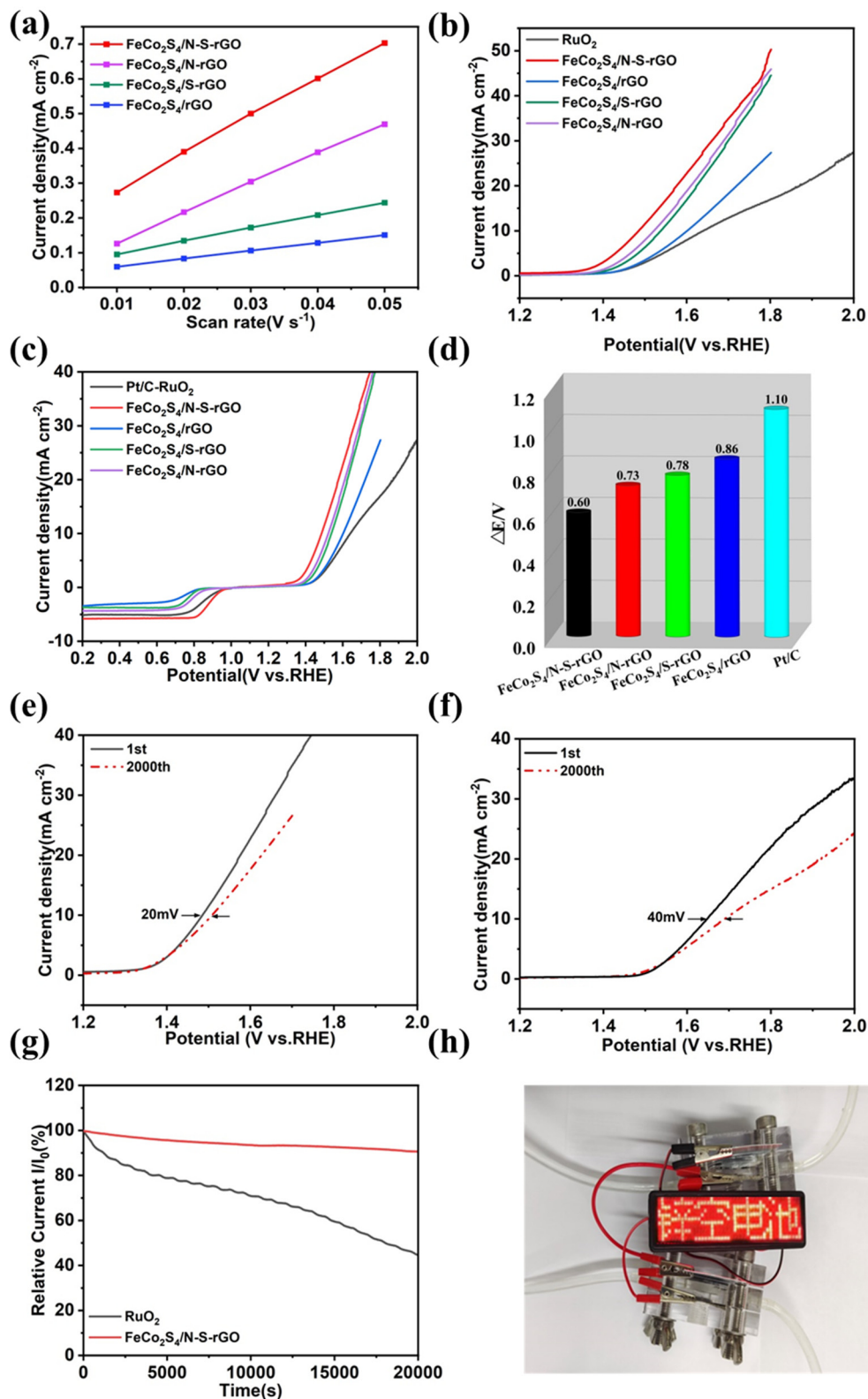
Figure S10. (a) The extraction of the C_{dl} of different catalysts; (b) LSV of different catalysts for OER; (c) ORR and OER polarization curves of different catalysts; (d) comparison of ΔE for different catalysts; (e) LSV curves of the $FeCo_2S_4$/N-S-rGO electrode before and after 2000 cycles; (f) LSV curves of the RuO_2 electrode before and after 2000 cycles; (g) timing current tests (i-t) for RuO_2 and $FeCo_2S_4$/N-S-rGO; (h) $FeCo_2S_4$/N-S-rGO applied to a series connected zinc-air battery pack to light up an LED display.
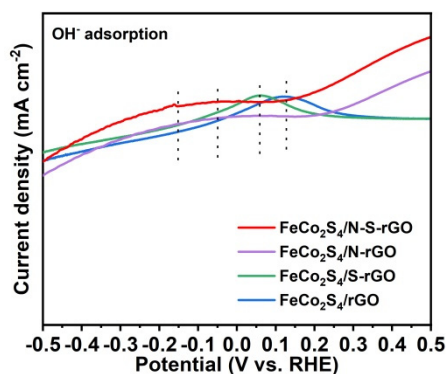
Figure S11. Oxidative LSV scans in N_2-bubbled 0.1 M NaOH of different catalysts.

Table S1. The proportion of the four types of nitrogen.

| Catalysts	pyridinic-N %	M-N %	pyrrolic-N %	graphitic-N %	oxidized-N %
FeCo2S4/N-S-rGO	35.0	15.6	13.8	25.7	9.9
FeCo2S4/N-rGO	23.8	12.5	27.8	20.4	15.5
N-S-rGO	32.1	-	34. 5	15.0	18.4

Table S2. Comparison of ORR and OER performance under 0.1 M KOH electrolyte in the literature.

Catalysts	E_{10} (V *vs.* RHE)	$E_{1/2}$ (V *vs.* RHE)	ΔE (V *vs.* RHE)	Ref.
FeCo2S4/N-S-rGO	1.490	0.890	0.600	This work
Co9S8/S-CNTs	1.561	0.810	0.751	[1]
NiCo2S4/N-CNT	1.600	0.800	0.800	[2]
Co3S4@N, S-rGO	1.700	0.760	0.940	[3]
Co/Co9S8@SNC-900	1.550	0.820	0.730	[4]
ZnCo2O4/N-CNT	1.660	0.870	0.790	[5]

$Co_{0.5}Fe_{0.5}S$@N-MC	1.620	0.808	0.812	[6]
Co_9S_8@SNC	1.550	0.846	0.704	[7]
CoFe/S-N-C	1.588	0.855	0.733	[8]
Fe-NC SAC	1.680	0.880	0.800	[9]
P-CoNi@NSCs	1.590	0.810	0.780	[10]
Mn-Co-Fe-N/S@CNT	1.616	0.807	0.809	[11]
Ag-$MnFe_2O_4$/NSPG	1.790	0.831	0.959	[12]
Ni_3S_2-QDs/SNC	1.540	0.864	0.676	[13]
Co-Ni-S@NSPC	1.700	0.820	0.880	[14]
$FeNi_3$@NC	1.51	0.860	0.650	[15]
ZnS/NSC-800	1.695	0.865	0.83	[16]
Ni-Co-S/NSC	1.540	0.810	0.730	[17]
Ni_3Fe/N-C sheet	1.620	0.780	0.840	[18]
Co_3O_4/N-rGO	1.720	0.790	0.930	[19]
Vs-$NiCo_2S_4$/N, S-rGO	1.570	0.840	0.730	[20]
$NiCoMnS_4$/N-rGO	1.640	0.820	0.820	[21]

References

1. Wang, J.L.; Liu, H.; Liu, Y.; Wang, W.H.; Sun, Q.; Wang, X.B.; Zhao, X.Y.; Hu, H.; Wu, M.B. Sulfur bridges between Co_9S_8 nanoparticles and carbon nanotubes enabling robust oxygen electrocatalysis. *Carbon* **2019**, *144*, 259-268, doi:10.1016/j.carbon.2018.12.031.

2. Han, X.P.; Wu, X.Y.; Zhong, C.; Deng, Y.D.; Zhao, N.Q.; Hu, W.B. $NiCo_2S_4$ nanocrystals anchored on nitrogen-doped carbon nanotubes as a highly efficient bifunctional electrocatalyst for rechargeable zinc-air batteries. *Nano Energy* **2017**, *31*, 541-550, doi:10.1016/j.nanoen.2016.12.008.

3. Liu, Q.; Jin, J.T.; Zhang, J.Y. $NiCO_2S_4$@graphene as a Bifunctional Electrocatalyst for Oxygen Reduction and Evolution Reactions. *ACS Appl. Mater. Interfaces* **2013**, *5*, 5002-5008, doi:10.1021/am4007897.

4. Zhang, Y.; Ma, J.L.; Ma, M.S.; Zhang, C.F.; Jia, X.L.; Wang, G.X. Co and Co_9S_8 nanoparticles uniformly embedded in S, N-doped porous carbon as electrocatalysts for rechargeable zinc-air batteries. *J. Mater. Res. Technol-JMRT* **2022**, *18*, 3764-3776, doi:10.1016/j.jmrt.2022.04.048.

5. Liu, Z.Q.; Cheng, H.; Li, N.; Ma, T.Y.; Su, Y.Z. $ZnCo_2O_4$ Quantum Dots Anchored on Nitrogen-Doped Carbon Nanotubes as Reversible Oxygen Reduction/Evolution Electrocatalysts. *Adv. Mater.* **2016**, *28*, 3777-3784, doi:10.1002/adma.201506197.

6. Shen, M.X.; Ruan, C.P.; Chen, Y.; Jiang, C.H.; Ai, K.L.; Lu, L.H. Covalent Entrapment of Cobalt-Iron Sulfides in N-Doped Mesoporous Carbon: Extraordinary Bifunctional Electrocatalysts for Oxygen Reduction and Evolution Reactions. *ACS Appl. Mater. Interfaces* **2015**, *7*, 1207-1218, doi:10.1021/am507033x.

7. Xu, F.F.; Zhao, J.H.; Wang, J.L.; Guan, T.T.; Li, K.X. Strong coordination ability of sulfur with cobalt for facilitating scale-up synthesis of Co9S8 encapsulated S, N co-doped carbon as a trifunctional electrocatalyst for oxygen reduction reaction, oxygen and hydrogen evolution reaction. *J. Colloid Interface Sci.* **2022**, *608*, 2623-2632, doi:10.1016/j.jcis.2021.10.182.

8. Li, G.J.; Tang, Y.B.; Fu, T.T.; Xiang, Y.; Xiong, Z.P.; Si, Y.J.; Guo, C.Z.; Jiang, Z.Q. S, N co-doped carbon nanotubes coupled with CoFe nanoparticles as an efficient bifunctional ORR/OER electrocatalyst for rechargeable Zn-air batteries. *Chem. Eng. J.* **2022**, *429*, 8, doi:10.1016/j.cej.2021.132174.

9. Du, C.; Gao, Y.J.; Wang, J.G.; Chen, W. A new strategy for engineering a hierarchical porous carbon-anchored Fe single-atom electrocatalyst and the insights into its bifunctional catalysis for flexible rechargeable Zn-air batteries. *J. Mater. Chem. A* **2020**, *8*, 9981-9990, doi:10.1039/d0ta03457f.

10. He, X.H.; Fu, J.; Niu, M.Y.; Liu, P.F.; Zhang, Q.; Bai, Z.Y.; Yang, L. Long-range interconnected nanoporous Co/Ni/C composites as bifunctional electrocatalysts for long-life rechargeable zinc-air batteries. *Electrochim. Acta* **2022**, *413*, 10, doi:10.1016/j.electacta.2022.140183.

11. Wang, K.L.; Liu, X.T.; Zuo, Y.Y.; Wei, M.H.; Xiao, Y.; Zhang, P.F.; Xiong, J.Y.; Pei, P.C. A Highly Active Bifunctional Catalyst of Mn-Co-Fe-N/S@CNT for Rechargeable Zinc-Air Batteries. *J. Electrochem. Soc.* **2021**, *168*, 7, doi:10.1149/1945-7111/ac3718.

12. Dong, H.Z.; Chen, Y.J.; Gong, C.; Sui, L.N.; Sun, Q.; Lv, K.L.; Dong, L.F. N, S, P-Codoped Graphene-Supported $Ag-MnFe_2O_4$ Heterojunction Nanoparticles as Bifunctional Oxygen Electrocatalyst with High Efficiency. *Catalysts* **2021**, *11*, 10, doi:10.3390/catal11121550.

13. Xu, F.F.; Wang, J.L.; Zhang, Y.X.; Wang, W.; Guan, T.T.; Wang, N.; Li, K.X. Structure-engineered bifunctional oxygen electrocatalysts with Ni_3S_2 quantum dot embedded S/N-doped carbon nanosheets for rechargeable Zn-air batteries. *Chem. Eng. J.* **2022**, *432*, 11, doi:10.1016/j.cej.2021.134256.

14. Fang, W.G.; Hu, H.B.; Jiang, T.T.; Li, G.; Wu, M.Z. N- and S-doped porous carbon decorated with in-situ synthesized Co-Ni bimetallic sulfides particles: A cathode catalyst of rechargeable Zn-air batteries. *Carbon* **2019**, *146*, 476-485, doi:10.1016/j.carbon.2019.01.027.

15. Chen, D.; Zhu, J.W.; Mu, X.Q.; Cheng, R.L.; Li, W.Q.; Liu, S.L.; Pu, Z.H.; Lin, C.; Mu, S.C. Nitrogen-Doped carbon coupled $FeNi_3$ intermetallic compound as advanced bifunctional electrocatalyst for OER, ORR and zn-air batteries. *Appl. Catal. B-Environ.* **2020**, *268*, 9, doi:10.1016/j.apcatb.2020.118729.

16. Peng, Y.Y.; Zhang, F.P.; Zhang, Y.L.; Luo, X.; Chen, L.; Shi, Y.L. ZnS modified N, S dual-doped interconnected porous carbon derived from dye sludge waste as high-efficient ORR/OER catalyst for rechargeable zinc-air battery. *J. Colloid Interface Sci.* **2022**, *616*, 659-667, doi:10.1016/j.jcis.2022.02.102.

17. Wu, Z.X.; Wu, H.B.; Niu, T.F.; Wang, S.; Fu, G.T.; Jin, W.; Ma, T.Y. Sulfurated Metal-Organic Framework-Derived Nanocomposites for Efficient Bifunctional Oxygen Electrocatalysis and Rechargeable Zn- Air Battery. *ACS Sustain. Chem. Eng.* **2020**, *8*, 9226-9234, doi:10.1021/acssuschemeng.0c03570.

18. Fu, G.T.; Cui, Z.M.; Chen, Y.F.; Li, Y.T.; Tang, Y.W.; Goodenough, J.B. Ni_3Fe-N Doped Carbon Sheets as a Bifunctional Electrocatalyst for Air Cathodes. *Adv. Energy Mater.* **2017**, *7*, 8, doi:10.1002/aenm.201601172.

19. Li, Y.B.; Zhong, C.; Liu, J.; Zeng, X.Q.; Qu, S.X.; Han, X.; Deng, Y.P.; Hu, W.B.; Lu, J. Atomically Thin Mesoporous Co_3O_4 Layers Strongly Coupled with N-rGO Nanosheets as High-Performance Bifunctional Catalysts for 1D Knittable Zinc-Air Batteries. *Adv. Mater.* **2018**, *30*, 9, doi:10.1002/adma.201703657.

20. Feng, X.T.; Jiao, Q.Z.; Li, Q.; Shi, Q.; Dai, Z.; Zhao, Y.; Li, H.S.; Feng, C.H.; Zhou, W.; Feng, T.Y. $NiCo_2S_4$ spheres grown on N,S co-doped rGO with high sulfur vacancies as superior oxygen bifunctional electrocatalysts. *Electrochim. Acta* **2020**, *331*, 11, doi:10.1016/j.electacta.2019.135356.https://doi.org/10.1016/j.electacta.2019.135356.

21. Pendashteh, A.; Sanchez, J.S.; Palma, J.; Anderson, M.; Marcilla, R. Anchored $NiCoMnS_4$ nanoparticles on N-doped rGO: High-performance bifunctional electrocatalysts for rechargeable Zn-Air batteries. *Energy Storage Mater.* **2019**, *20*, 216-224, doi:10.1016/j.ensm.2019.04.018.